

QUIET SUN INTERNETWORK MAGNETIC FIELDS FROM THE INVERSION OF *Hinode* MEASUREMENTS

D. OROZCO SUÁREZ¹, L.R. BELLOT RUBIO¹, J.C. DEL TORO INIESTA¹, S. TSUNET², B.W. LITES³, K. ICHIMOTO², Y. KATSUKAWA², S. NAGATA⁴, T. SHIMIZU⁵, R.A. SHINE⁶, Y. SUEMAT², T.D. TARBELL⁶, A.M. TITLE⁶

To appear in ApJ Letters

ABSTRACT

We analyze Fe I 630 nm observations of the quiet Sun at disk center taken with the spectropolarimeter of the Solar Optical Telescope aboard the *Hinode* satellite. A significant fraction of the scanned area, including granules, turns out to be covered by magnetic fields. We derive field strength and inclination probability density functions from a Milne-Eddington inversion of the observed Stokes profiles. They show that the internetwork consists of very inclined, hG fields. As expected, network areas exhibit a predominance of kG field concentrations. The high spatial resolution of *Hinode*'s spectropolarimetric measurements brings to an agreement the results obtained from the analysis of visible and near-infrared lines.

Subject headings: Sun: magnetic fields – Sun: photosphere – Instrumentation: high angular resolution

1. INTRODUCTION

Most of the studies aimed at determining the distribution of field strengths in the internetwork (IN) quiet Sun have used polarimetric measurements in the spectral regions around 630 nm and 1565 nm, but their results do not agree. The visible Fe I lines at 630.2 nm indicate a predominance of kG fields (Sánchez Almeida & Lites 2000; Domínguez Cerdeña et al. 2003; Socas-Navarro & Lites 2004), whereas the infrared lines at 1565 nm suggest hG fields (Lin 1995; Lin & Rimele 1999; Khomenko et al. 2003; Martínez González et al. 2006a; Domínguez Cerdeña et al. 2006). The distribution of IN field inclinations has only been studied by Lites et al. (1996) and Khomenko et al. (2003).

Here we analyze Fe I 630 nm measurements of the quiet Sun taken by the spectropolarimeter aboard *Hinode* at the unprecedented spatial resolution of 0".32. The observed Stokes spectra are inverted to determine the distribution of field strengths and inclinations in the observed region. Our results show that most of the IN fields are weak, opposite to what has been found from ground-based measurements of the same lines at 1".

2. OBSERVATIONS

A quiet solar region of 302"×162" was observed at disk center on March 10, 2007 using the spectropolarimeter (SP; Lites et al. 2001) aboard *Hinode* (Kosugi et al. 2007). The SP records the Stokes spectra of the Fe I 630.2 nm lines with a wavelength sampling of 2.15 pm pixel⁻¹ and a scanning step of 0".1476. We used an exposure time of 4.8 s per slit position, resulting

in a noise level of $1.2 \times 10^{-3} I_c$ in Stokes Q and U , and $1.1 \times 10^{-3} I_c$ in Stokes V . The data have been corrected for dark current, flat-field, and instrumental cross-talk as explained by Lites et al. (2007c).

The scanned area covers both network and internetwork regions. The rms intensity contrast of the granulation is about 7.5%, which represents the highest angular resolution ever obtained in spectropolarimetric studies of the quiet Sun. A visual inspection of the circular and linear polarization maps reveals a wealth of magnetic signals in the field of view (FOV). We estimate that 87.1% and 35.5% of the image show polarization signals larger than 3 and 4.5 times the noise level, respectively.

3. INVERSION STRATEGY

To derive the vector magnetic field from the observed Stokes profiles we use a least-square inversion technique based on Milne-Eddington (ME) atmospheres. We assume a one-component, laterally homogeneous atmosphere together with stray/scattered light contamination. The inversion returns the values of 10 free parameters, including the three components of the magnetic field (strength, inclination, and azimuth) and the stray light factor, α . The stray light intensity profile is evaluated individually for each pixel by averaging Stokes I within a box 1" wide centered on the pixel. We do not consider broadening of the spectra by macroturbulent velocities. The inversion is applied to the Fe I 630.15 and 630.25 nm lines simultaneously, using a Gaussian of 2.5 pm FWHM to account for the spectral resolving power of the SP.

Orozco Suárez et al. (2007a) demonstrated that this strategy results in accurate magnetic field inferences for fields above 100 G. The field strengths derived from ME inversions of Fe I 630 nm measurements at 0".32 resolution are very similar to those present around optical depth $\tau_5 = 0.01$, with rms uncertainties not larger than 150 G. ME inversions turn out to be largely independent of the noise and field strength initialization, provided they are run on pixels showing polarization signals above a reasonable threshold (Orozco Suárez et al. 2007b). Here we only analyze pixels with Stokes Q , U or V amplitudes larger than 4.5 times their noise levels,

¹ Instituto de Astrofísica de Andalucía (CSIC), Apdo. de Correos 3004, 18080 Granada, Spain

² National Astronomical Observatory of Japan, 2-21-1 Osawa, Mitaka, Tokyo 181-8588, Japan

³ High Altitude Observatory, NCAR, 3080 Center Green Dr. CG-1, Boulder, CO 80301, USA

⁴ Hida Observatory, Kyoto University, Takayama, Gifu 506-1314, Japan

⁵ Institute of Space and Astronautical Science, JAXA, Sagami-hara, Kanagawa 229-8510, Japan

⁶ Lockheed Martin Solar and Astrophysics Laboratory, Bldg. 252, 3251 Hanover St., Palo Alto, CA 94304, USA

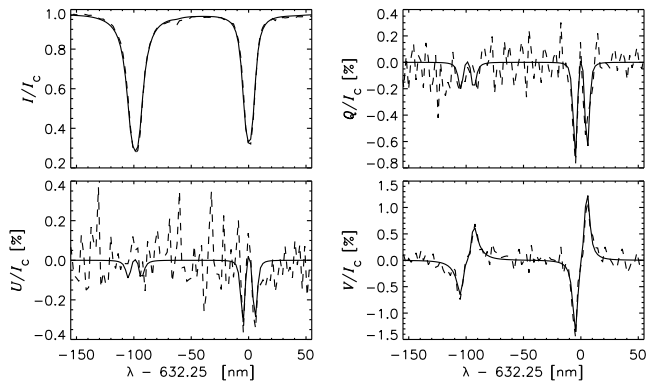


FIG. 1.— Observed (*dashed*) and best-fit (*solid*) Stokes profiles emerging from a IN pixel. The field strength and the stray light factor are 177 G and 58%, respectively.

in order to exclude profiles which cannot be inverted reliably. This threshold corresponds to an apparent flux density⁷ of 13.4 Mx cm^{-2} .

Figure 1 shows a sample fit for an individual pixel belonging to the IN. In this case, the inversion retrieves a field strength of 177 G and a field inclination of 106° . Of interest is that the pixel shows clear Stokes Q and U signals above the noise, just as many other IN positions. Additional examples can be found in Orozco Suárez et al. (2007b).

4. RESULTS

Figure 2 shows maps of the retrieved field strength and inclination for a small portion of the observed area. Black regions represent pixels which have not been analyzed because of their small signals. In the field strength map two different regions can be identified: the network, characterized by strong fields (above 1 kG), and the IN, with much weaker fields. Supergranular cells are clearly outlined by the network fields. The inclination map shows that network flux concentrations exhibit nearly vertical fields in their interiors and more inclined fields toward the edges, suggesting the presence of magnetic canopies. By contrast, IN fields are rather horizontal.

The mean unsigned apparent flux density in the FOV is 16.7 Mx cm^{-2} , of which 9.5 Mx cm^{-2} correspond to longitudinal flux and 11.3 Mx cm^{-2} to transverse flux⁸. In IN regions we find a mean flux density of 8.4 Mx cm^{-2} , with 3.4 Mx cm^{-2} corresponding to longitudinal flux and 7.1 Mx cm^{-2} to transverse flux. The large occurrence of horizontal fields confirms the discovery of strong linear polarization signals by Lites et al. (2007a,b). The net flux density is 1.7 Mx cm^{-2} in the full FOV and -0.1 Mx cm^{-2} in the IN.

The bottom panels of Fig. 2 represent a zoom over a $7''.4 \times 7''.4$ IN area (white box in the top images) and display continuum intensities, magnetic field strengths, field inclinations, and total polarization signals. In the field

strength map one can see that most of the fields are weak. The stronger concentrations are located in intergranular lanes (the contours outline the granulation). Interestingly, we find ubiquitous weak fields over granules. The rightmost map just confirms this finding. Note also that the fields are more horizontal in granular regions than elsewhere.

4.1. Field strength and inclination distributions

Figure 3 shows probability density functions (PDFs) for the magnetic field strength (*left*) and field inclination (*right*). The solid lines represent total PDFs considering the $\sim 650\,000$ pixels inverted. The upper panels display PDFs for granules (*dotted*) and intergranular lanes (*dashed*). The separation between granular and intergranular regions has been performed using the continuum intensity and the inferred line-of-sight velocity. The bottom panels compare the PDFs of IN regions (*dashed*) with those calculated from the magneto-convection simulations of Vögler et al. (2005), for a snapshot with mean unsigned flux of 10 Mx cm^{-2} (*dot-dashed*). IN areas have been selected manually, excluding the boundaries of supergranular cells on purpose.

The peak of the total PDF for the field strength is located at about 90 G. The curve decreases rapidly toward stronger fields: at around 1 kG it reaches a minimum and then shows a small hump centered at about 1.4 kG. Strong fields ($B > 1 \text{ kG}$) are found in only 4.5% of the pixels, the majority of which correspond to network areas. It is important to emphasize that the PDF does not increase monotonically from 90 G to 0 G. This suggests that the inversions are not biased by noise, and that the peak at 90 G is likely solar in origin.

The upper left panel of Fig. 3 shows a steeper field strength distribution in granules as compared with intergranular lanes, i.e., strong fields are much less abundant in granular regions. Noticeable is the large fraction of very inclined ($\sim 90^\circ$) fields in granules. Although inclined fields are also common in downdrafts, the field lines tend to be more horizontal over convective upflows (upper right panel of Fig. 3). The rapid increase of the PDF near 0° and 180° , however, indicates that vertical fields also exist in granules.

In the IN, the field strength distribution reaches a maximum near 90 G and decreases toward larger fields (bottom left panel of Fig. 3). This demonstrates that the IN basically consists of hG flux concentrations. In the range 1-8 hG, the PDF is well described by a lognormal function $f(B) = (\pi^{1/2}\sigma B)^{-1} \exp[-(\ln B - \ln B_0)^2/\sigma^2]$ with $B_0 = 36.7 \text{ G}$ and $\sigma = 1.2$. The shapes of the field strength distributions derived from the simulations and the IN measurements are surprisingly similar. By contrast, the field inclination PDFs appear to be rather different, being much flatter in the simulations (Fig. 3, bottom right panel).

4.2. Stray-light factor distribution

Figure 4 shows the stray-light factor PDF for the full FOV and IN regions. Both of them peak at $\alpha \sim 0.8$. For reasons explained in Orozco Suárez et al. (2007b), we interpret the stray light contamination as a degradation of the polarization signals due to diffraction, but it might also represent filling factors different from 1. In that

⁷ The apparent flux density has been calculated by determining the magnetic parameters of a ME atmosphere with vertical fields that produces Stokes V signals at the level of the noise. The thermodynamic parameters of the model have been fixed to the mean values derived from the Hinode measurements.

⁸ The mean flux densities are computed over the FOV assigning zero fluxes to pixels which were not inverted, so they represent lower limits.

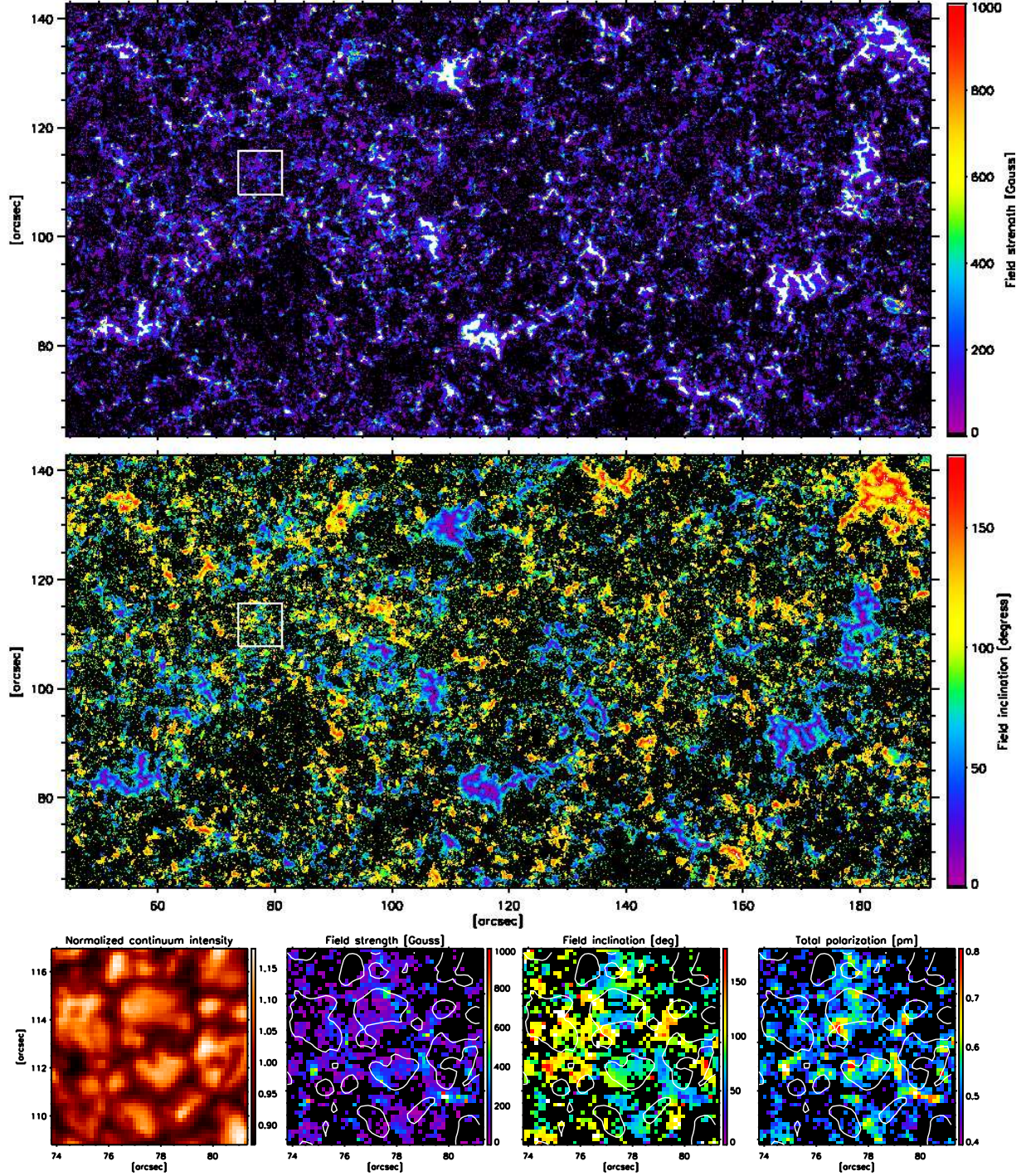


FIG. 2.— Small area of $148'' \times 74''$ showing the magnetic field strengths (*top*) and inclinations (*middle*) inferred from the inversion. Network and internetwork areas can be easily identified. Black areas correspond to non-inverted pixels. The field strength color bar has been clipped at 1000 G (*white*). The four bottom panels represent a small IN area of $7.4'' \times 7.4''$ (white box in the upper panels). They display continuum intensities, magnetic field strengths, field inclinations, and total polarization signals, $\int (Q^2 + U^2 + V^2)^{1/2} d\lambda / I_c^{\text{QS}}$. Contour lines represent regions with continuum intensities $I_c / I_c^{\text{QS}} > 1.05$.

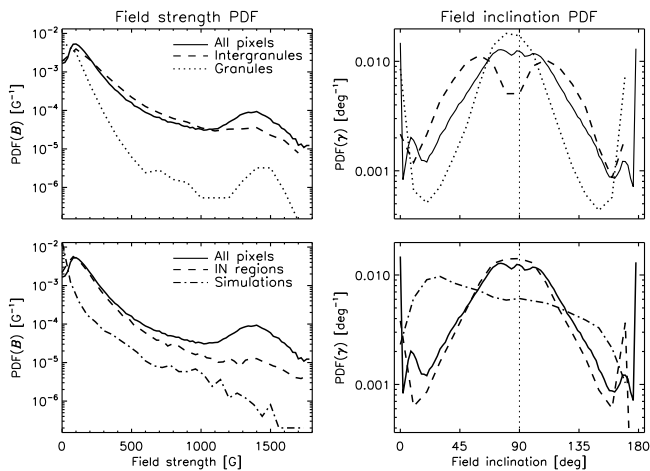


FIG. 3.— Magnetic field strength (*left*) and inclination (*right*) probability density functions. In the upper panels, the solid, dashed, and dotted lines stand for all pixels in the FOV, intergranular lanes, and granules. In the bottom panels, the solid and dashed lines represent all pixels in the FOV and IN regions, respectively. Dot-dashed lines show PDFs from magneto-convection simulations with mean flux density of 10 Mx cm^{-2} .

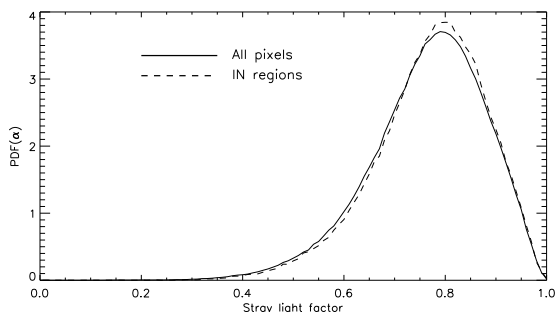


FIG. 4.— PDF of the stray light factor. Solid and dashed lines represent the full FOV and IN regions, respectively.

case, the average fractional area of the pixel occupied by magnetic fields (given by $1 - \alpha$) would be small, showing a peak at 0.2.

Errors in the stray light determination would immediately lead to different field strengths and/or inclinations because most of the observed signals are formed in the weak-field regime. The high-spatial resolution allowed by the *Hinode* SP, however, makes it possible to distinguish between field strength and stray-light factor unambiguously, even under weak field conditions. The key ingredient is Stokes *I*: the intensity profile is very sensitive to small variations in stray-light contamination. Orozco

Suárez et al. (2007b) have demonstrated that, in practice, the inversion code uses Stokes *I* to determine the stray light factor. For more details, including an analysis of the χ^2 merit function minimized by the code, the interested reader is referred to their Sect. 6.

5. DISCUSSION AND CONCLUSIONS

The high spatial resolution spectropolarimetric measurements of *Hinode* indicate that most IN fields are weak. This is in agreement with the picture derived from the more magnetically sensitive Fe I lines at 1565 nm (Lin 1995; Collados 2001; Khomenko et al. 2003; Martínez González et al. 2006b) and from lines showing hyperfine structure such as Mn I 553 nm (López Ariste et al. 2006) and Mn I 1526.2 nm (Asensio Ramos et al. 2007). Keller et al. (1994) also found weak fields in the internetwork using the Fe I 525.0 nm lines, although at a lower spatial resolution and without inclination information. Our results seem to confirm the mean IN field strength of $\sim 100 \text{ G}$ derived by Trujillo Bueno et al. (2004) from a Hanle-effect interpretation of Sr I 460.7 nm measurements.

Interestingly, the slope of the field strength distribution in the IN is similar to that obtained from magneto-convection simulations of comparable mean flux density. The observed field inclinations, however, turn out to be significantly larger than those predicted by the simulations. The scenario of an IN filled by nearly horizontal hG fields is compatible with the large trasverse magnetic fluxes found in the IN by Lites et al. (2007a,b). We still do not know the origin of such ubiquitous horizontal IN fields, but Lites et al. (2007b) have suggested a number of plausible mechanisms.

In summary, Milne-Eddington inversions of the Fe I 630 nm lines observed by *Hinode* at $0'32$ reveal a predominance of hG fields in quiet Sun internetwork regions, contrary to what is obtained from the same lines at $1''$. This is the first time that Fe I 630 nm observations confirm the weak IN fields indicated by near-infrared measurements, which may definitely close the discrepancy between the results derived from both spectral regions.

Hinode is a Japanese mission developed and launched by ISAS/JAXA, with NAOJ as domestic partner and NASA and STFC (UK) as international partners. It is operated by these agencies in collaboration with ESA and NSC (Norway). This work has been partially funded by the Spanish Ministerio de Educación y Ciencia through project ESP2006-13030-C06-02.

REFERENCES

- Asensio Ramos, A., Martínez González, M. J., López Ariste, A., Trujillo Bueno, J., & Collados, M. 2007, *ApJ*, 659, 829
 Collados, M. 2001, in: *Advanced Solar Polarimetry – Theory, Observation, and Instrumentation*, ASP Conf. Series, 236, 255
 Domínguez Cerdeña, I., Kneer, F., & Sánchez Almeida, J. 2003, *ApJ*, 582, L55
 Domínguez Cerdeña, I., Almeida, J. S., & Kneer, F. 2006, *ApJ*, 646, 1421
 Keller, C. U., Deubner, F.-L., Egger, U., Fleck, B., & Povel, H. P. 1994, *A&A*, 286, 626
 Khomenko, E.V., Collados, M., Solanki, S.K., Lagg, A., & Trujillo Bueno, J. 2003, *A&A*, 408, 1115
 Kosugi, T., et al. 2007, *Sol. Phys.*, in press
 Lin, H. 1995, *ApJ*, 446, 421
 Lin, H., & Rimmele, T. 1999, *ApJ*, 514, 448
 Lites, B.W., Leka, K.D., Skumanich, A., Martínez Pillet, V., & Shimizu, T. 1996, *ApJ*, 460, 1019
 Lites, B. W., Elmore, D. F., & Stenander, K. V. 2001, *ASP Conf. Ser.*, 236, 33
 Lites, B.W., et al. 2007a, *PASJ*, in press
 Lites, B.W., et al. 2007b, *ApJ*, submitted
 Lites, B.W., et al. 2007c, *Sol. Phys.*, in preparation
 López Ariste, A., Tomczyk, S., & Casini, R. 2006, *A&A*, 454, 663
 Martínez González, M.J., Collados, M., & Ruiz Cobo, B. 2006a, *A&A*, 456, 1159

- Martínez González, M. J., Collados, M., & Ruiz Cobo, B. 2006b, ASP Conf. Series, 358, 36
- Orozco Suárez, D., Bellot Rubio, L.R. & del Toro Iniesta, J.C. 2007a, ApJ, 662, L31
- Orozco Suárez, D., et al. 2007b, PASJ, in press (astro-ph/0709.2033)
- Sánchez Almeida, J., & Lites, B.W. 2000, ApJ, 532, 1215
- Socas-Navarro, H., & Lites, B. W. 2004, ApJ, 616, 587
- Trujillo Bueno, J., Shchukina, N., & Asensio Ramos, A. 2004, Nature, 430, 326
- Vögler, A., Shelyag, S., Schüssler, M., Cattaneo, F., Emonet, T., & Linde, T. 2005, A&A, 429, 335